

# Natural Image Segmentation with Adaptive Texture and Boundary Encoding <sup>\*</sup>

Shankar R. Rao<sup>1</sup>, Hossein Mobahi<sup>1</sup>, Allen Y. Yang<sup>2</sup>,  
S. Shankar Sastry<sup>2</sup>, and Yi Ma<sup>1,3</sup>

<sup>1</sup> Coordinated Science Laboratory, University of Illinois at Urbana-Champaign  
{srrao,hmobahi2,yima}@illinois.edu

<sup>2</sup> EECS Department, University of California, Berkeley  
{yang,sastry}@eecs.berkeley.edu

<sup>3</sup> Visual Computing Group, Microsoft Research Asia, Beijing, China

**Abstract.** We present a novel algorithm for unsupervised segmentation of natural images that harnesses the principle of minimum description length (MDL). Our method is based on observations that a homogeneously textured region of a natural image can be well modeled by a Gaussian distribution and the region boundary can be effectively coded by an adaptive chain code. The optimal segmentation of an image is the one that gives the shortest coding length for encoding all textures and boundaries in the image, and is obtained via an agglomerative clustering process applied to a hierarchy of decreasing window sizes. The optimal segmentation also provides an accurate estimate of the overall coding length and hence the true entropy of the image. Our algorithm achieves state-of-the-art results on the Berkeley Segmentation Dataset compared to other popular methods.

## 1 Introduction

The task of partitioning a natural image into regions with homogeneous texture, commonly referred to as *image segmentation*, is often a crucial first step for high-level image understanding, significantly reducing the complexity of content analysis of images. Image segmentation and its higher-level applications are largely designed to emulate functionalities of human visual perception (e.g., object recognition and scene understanding), and hence dominant criteria for measuring segmentation performance are based on qualitative and quantitative comparisons with human segmentation results. In the literature, investigators have explored several important models and principles that can lead to good image segmentation:

1. Different texture regions of a natural image admit a mixture model [1]. For example, Normalized Cuts (NC) [2] and F&H [3] formulate the segmentation as a graph-cut problem, while Mean Shift (MS) [4] seeks a partition of a color image based on different modes within the estimated empirical distribution.

---

<sup>\*</sup> This work is partially supported by NSF CAREER IIS-0347456, ONR YIP N00014-05-1-0633, and ARO MURI W911NF-06-1-0076.

2. Region contours/edges convey important information about the saliency of the objects in the image and their shapes [5–7]. Several recent methods have been proposed to combine the cues of homogeneous color and texture with the cue of contours in the segmentation process [8, 9].
3. The properties of local features (including texture and edges) usually do not share the same level of homogeneity at the same spatial scale. Thus, salient image regions can only be extracted from a hierarchy of image features under multiple resolutions [10–12].

Despite much work in this area, good image segmentation remains elusive to obtain for practitioners, mainly for the following two reasons: 1. There is little consensus on what criteria should be used to evaluate the quality of image segmentations. It is difficult to strike a good balance between objective measures that depend solely on the intrinsic statistics of imagery data and subjective measures that try to empirically model human perception. 2. In the search for objective measures, there has been a lack of consensus on good models for a unified representation of image segments including both their textures and contours.

Recently an *objective* metric based on the notion of lossy *minimum description length* (MDL) has been proposed for evaluating clustering of general mixed data [13]. The basic idea is that, given a potentially mixed data set, the “optimal segmentation” is the one that, over all possible segmentations, minimizes the coding length of the data, subject to a given quantization error. For data drawn from a mixture of Gaussians, the optimal segmentation can often be found efficiently using an agglomerative clustering approach. The MDL principle and the new clustering method have later been applied to the segmentation of natural images, known as *compression-based texture merging* (CTM) [12]. Preliminary success of this approach leads to the following important question: *To what extent is segmentation obtained by image compression consistent with human perception?*

However, although the CTM method utilizes the idea of data compression, it does not exactly seek to compress the image *per se*. First, it “compresses” feature vectors or windows extracted around all pixels by grouping them into clusters as a mixture of Gaussian models. As a result, the final coding length is highly *redundant* due to severe overlap between windows of adjacent pixels, and has no direct relation to the true entropy of the image. Second, the segmentation result encodes the membership of pixels using a Huffman code that does not take into account of spatial adjacency of pixels nor smoothness of boundaries. Thus, CTM does not give a good estimate of the true entropy of the image and its success cannot be used to justify a strong connection between image segmentation and image compression.

*Contributions.* In this paper, we contend that, much better segmentation results can be obtained if we follow more closely the principle of image compression, by correctly counting only the necessary bits needed to encode a natural image for both the texture and boundaries. The proposed algorithm precisely estimates

the coding length needed to encode the texture of each region based on the rate distortion of its probabilistic distribution and the number of *non-overlapping* windows inside. In order to adapt to the different scales and shapes of texture regions in the image, a hierarchy of multiple window sizes is incorporated in the segmentation process. The algorithm further encodes the boundary information of each homogeneous texture region by carefully counting the number of bits needed to encode the boundary with an adaptive chain code.

Based on the MDL principle, the optimal segmentation of an image is defined as the one that minimizes its total coding length, in this case a close approximation to the true entropy of the image. With any fixed quantization, the final coding length gives a purely objective measure for how good the segmentation is in terms of the level of image compression. We conduct extensive experiments to compare the results with human segmentation, using the Berkeley Segmentation Dataset (BSD) [14]. Although our method is conceptually simple and the measure used is purely objective, the segmentation results match extremely well with those by human, exceeding or competing with the best segmentation algorithms. The source code of our algorithm, as well as a detailed report of the segmentation results are available online at [http://perception.csl.illinois.edu/coding/image\\_segmentation/](http://perception.csl.illinois.edu/coding/image_segmentation/).

## 2 Adaptive Texture and Boundary Encoding

In this section, we present a unified information-theoretic framework to encode both the texture and boundary information of a natural image. The implementation of the algorithm for adaptive image segmentation and the experiments to validate its performance will be presented in Sections 3 and 4.

### 2.1 Constructing Texture Vectors

We discuss how to construct texture vectors that represent homogeneous textures in image segments. Given an image in *RGB* format, we convert it to the  $L^*a^*b^*$  color space. It has been noted in the literature that such a color metric better approximates the perceptually uniform color space. In order to capture the variation of a local *texon*, one can directly apply a  $w \times w$  cut-off window around a pixel across the three color channels, and stack the color values inside the window in a vector form as in [12].

Figure 1 (left) illustrates our process for constructing features. Let the  $w$ -neighborhood  $\mathcal{W}_w(p)$  be the set of all pixels in a  $w \times w$  window centered at pixel  $p$ . We construct a set of features  $X$  by taking the  $w$ -neighborhood around each pixel in  $I$ , and then stacking each window as a column vector:

$$X \doteq \{\mathbf{x}_p \in \mathbb{R}^{3w^2} : \mathbf{x}_p = \mathcal{W}_w(p)^S \text{ for } p \in I\}. \quad (1)$$

For ease of computation, we reduce the dimensionality of these features by projecting the set of all features  $X$  onto their first  $D$  principal components. We

denote the set of features with reduced dimensionality as  $\hat{X}$ . We have observed that for many natural images, the first eight principal components of  $X$  contain over 99% of the energy. In this paper, we choose to assign  $D = 8$ .

Over the years, there have been many proposed methods to model the representation of image textures in natural images. One model that has been shown to be successful in encoding textures both empirically and theoretically is the Gaussian *Mesh Markov Model* (MMM) [15]. Particularly in texture synthesis, the Gaussian MMM provides consistent estimates of the joint distribution of the pixels in a window, which then can be used to fill in missing texture patches via a simple nonparametric scheme [16].

However, to determine the optimal compression rate for samples from a distribution, one must know the rate-distortion function of that distribution [12]. Unfortunately, the rate-distortion function for MMMs is, to our knowledge, not known in closed form, and difficult to estimate empirically. Over all distributions with the same variance, it is known that the Gaussian distribution will have the highest rate-distortion, and is in this sense, the worst case distribution for compression. Thus by using the rate-distortion for a Gaussian distribution, we obtain an upper bound for the true coding length of the MMM.

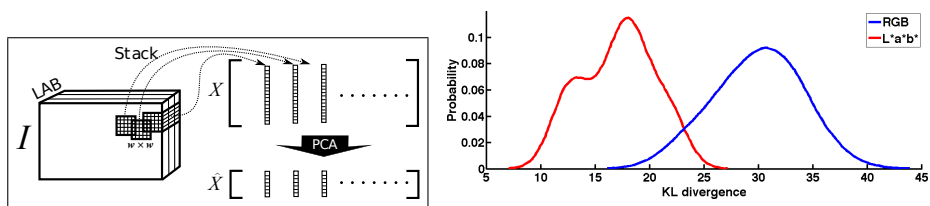


**Fig. 1. Left:** We construct features by stacking  $w \times w$  windows around all pixels of a  $L^*a^*b^*$  image  $I$  into a data matrix  $X$  and then using PCA. **Right:** (color) KL divergence of  $RGB$  and  $L^*a^*b^*$  windows from a true Gaussian distribution.

In the following, we provide an empirical experiment to determine in which color space ( $RGB$  or  $L^*a^*b^*$ ) feature windows from a region with homogeneous texture are better fit by a Gaussian distribution. We use as the ground truth training images from the BSD that were manually segmented by humans. Given the feature vectors within each region, we model the distribution both parametrically and non-parametrically. The parametric model  $Q$  is a multivariate normal distribution whose parameters are estimated from the samples using maximum likelihood. The non-parametric model  $P$  is obtained by kernel density estimation. If the true distribution is indeed normal, then  $P$  and  $Q$  should be very similar. Thus the KL divergence  $D_{KL}(P \parallel Q)$  can be used to measure the non-Gaussianity of the distribution. The overall non-Gaussianity of each image is simply the average of the non-Gaussianity over all regions. We repeat the above procedure for the entire manually segmented image dataset and estimate the distribution of KL divergence by kernel density estimation for  $RGB$  and  $L^*a^*b^*$

spaces. As Figure 1 (right) shows, between the two color metrics,  $L^*a^*b^*$  has lower mean and standard deviation and hence is better modeled by a Gaussian distribution.

## 2.2 Adaptive Texture Encoding

We now describe encoding the texture vectors based on the lossy MDL principle. First, we consider a single region  $R$  with  $N$  pixels. Based on [12], for a fixed quantization error  $\varepsilon$ , the expected number of bits needed to code the set of  $N$  feature windows  $\hat{X}$  up to distortion  $\varepsilon^2$  is given by:

$$L_\varepsilon(\hat{X}) \doteq \underbrace{\frac{D}{2} \log_2 \det(I + \frac{D}{\varepsilon^2} \Sigma)}_{\text{codebook}} + \underbrace{\frac{N}{2} \log_2 \det(I + \frac{D}{\varepsilon^2} \Sigma)}_{\text{data}} + \underbrace{\frac{D}{2} \log_2(1 + \frac{\|\boldsymbol{\mu}\|^2}{\varepsilon^2})}_{\text{mean}}, \quad (2)$$

where  $\boldsymbol{\mu}$  and  $\Sigma$  are the mean and covariance of the feature windows in  $\hat{X}$ . Equation (2) is the sum of three coding-lengths: the  $D$  Gaussian principal vectors as the codebook, the  $N$  windows w.r.t. that codebook, and the mean of the Gaussian distribution.

The coding length function (2) is uniquely determined by the mean and covariance ( $\boldsymbol{\mu}, \Sigma$ ). To estimate them empirically, we need to exclude the windows that cross the boundary of  $R$  (as shown in Figure 2). Such windows contain textures from the adjacent regions, which cannot be well modeled by a single Gaussian as the interior windows. Hence, the empirical mean  $\hat{\boldsymbol{\mu}}_w$  and covariance  $\hat{\Sigma}_w$  of  $R$  are only estimated from the *interior* of  $R$ :

$$\mathcal{I}_w(R) \doteq \{p \in R : q \in R, \forall q \in \mathcal{W}_w(p)\}. \quad (3)$$

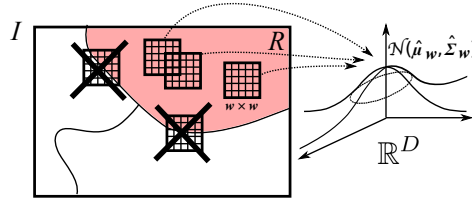


**Fig. 2.** Only windows from the interior of a region are used to compute  $\hat{\boldsymbol{\mu}}_w$  and  $\hat{\Sigma}_w$ .

Furthermore, in (2), encoding all texture vectors in  $\hat{X}$  to represent region  $R$  is highly redundant because the  $N$  windows *overlap* with each other. Thus, to obtain an efficient code of  $R$  that closely approximates its true entropy, we only need to code the *nonoverlapping* windows that can tile  $R$  as a grid. Ideally, if  $R$  is a rectangular region of size  $mw \times nw$ , where  $m$  and  $n$  are positive integers, then clearly we can tile  $R$  with exactly  $mn = \frac{N}{w^2}$  windows. So for coding the region  $R$ , (2) becomes:

$$L_{w,\varepsilon}(R) \doteq (\frac{D}{2} + \frac{N}{2w^2}) \log_2 \det(I + \frac{D}{\varepsilon^2} \hat{\Sigma}_w) + \frac{D}{2} \log_2(1 + \frac{\|\hat{\boldsymbol{\mu}}_w\|^2}{\varepsilon^2}). \quad (4)$$

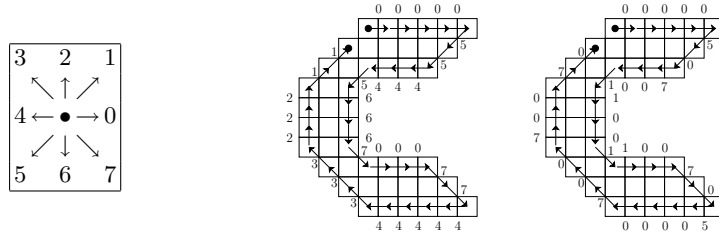


**Fig. 3. Left:** The Freeman chain code of an edge orientation along 8 possible directions. **Middle:** Representation of the boundary of a region in an image w.r.t. the Freeman chain code. **Right:** Representation w.r.t the difference chain code.

Real regions in natural images normally do not have such nice rectangular shapes. However, (4) remains a good approximation to the actual coding length of a region  $R$  with relatively smooth boundaries.<sup>4</sup>

### 2.3 Adaptive Boundary Encoding

To code windows from multiple regions in an image, one must know to which region each window belongs, so that each window can be decoded w.r.t. the correct codebook. For generic samples from multiple classes, one can estimate the distribution of each class label and then code the membership of the samples using a scheme that is asymptotically optimal for that class distribution (i.e., the Huffman code used in [12]). Such coding schemes are highly inefficient for natural image segmentation, as they do not leverage the spatial correlation of pixels in the same region. In fact, for our application, pixels from the same region form a connected component. Thus, a more efficient way of coding group membership for regions in images is to code the *boundary* of the region containing the pixels.

A well-known scheme for representing boundaries of image regions is the *Freeman chain code*. In this coding scheme, the orientation of an edge is quantized along 8 discrete directions, shown in Figure 3 (left). Let  $\{o_t\}_{t=1}^T$  denote the orientations of the  $T$  boundary edges of  $R$ . Since each chain code can be encoded using three bits, the coding length of the boundary of  $R$  is

$$B(R) = 3 \sum_{i=0}^7 \#(o_t = i). \tag{5}$$

The coding length  $B(R)$  can be further improved by using an adaptive Huffman code that leverages the prior distribution of the chain codes. Though the distribution of chain codes is essentially uniform in most images, for regions

<sup>4</sup> We briefly explain why (4) is a good approximation for the entropy of a large region with smooth boundary. In this case, the number of boundary-crossing windows is much smaller than the number of interior windows. The average coding length of boundary-crossing windows is then roughly proportional to the number pixels inside the region if the Gaussian distribution is sufficiently isotropic.

with smooth boundaries, we expect that the orientations of consecutive edges are similar, and so consecutive chain codes will not differ by much. Given an initial orientation (expressed in chain code)  $o_t$ , the *difference chain code* of the following orientation  $o_{t+1}$  is  $\Delta o_t \doteq \text{mod}(o_t - o_{t+1}, 8)$ . Figure 3 compares the original Freeman chain code with the difference chain code for representing the boundary of a region. Notice for this region, the difference encoding uses only half of the possible codes, with most being zeroes, while the Freeman encoding uses all eight chain codes. Given the prior distribution  $P[\Delta o]$  of difference chain codes,  $B(R)$  can be encoded more efficiently using a lossless Huffman coding scheme:

$$B(R) = - \sum_{i=0}^7 \#(\Delta o_t = i) \log_2(P[\Delta o = i]). \quad (6)$$

For natural images, we estimate  $P[\Delta o]$  using natural images from the BSD that were manually segmented by humans. We compare our distribution with one estimated by Liu and Zalik [17], who used 1000 images of curves, contour patterns and shapes obtained from the web. As seen in Table 1, over 58% of the difference chain codes obtained from manual segmentation of the BSD are zeroes, corresponding to no change in angle along the boundary. Thus, regions of natural images tend to have smoother boundaries when segmented by humans.

**Table 1.** The prior probability of the difference chain codes estimated from the BSD and by Liu and Zalik [17].

Difference Code	0	1	2	3	4	5	6	7
Angle change	0°	45°	90°	135°	180°	-135°	-90°	-45°
Probability (BSD)	0.585	0.190	0.020	0.000	0.002	0.003	0.031	0.169
Probability (Liu-Zalik)	0.453	0.244	0.022	0.006	0.003	0.006	0.022	0.244

### 3 Image Segmentation Algorithm

In this section, we show how to use the coding length functions we developed in Section 2 to construct a better compression-based image segmentation algorithm. We describe the basic approach below, and then propose a hierarchical scheme to deal with small and/or thin regions.

#### 3.1 Segmentation by Minimizing Coding Length

Suppose an image  $I$  can be segmented into non-overlapping regions  $\mathcal{R} = \{R_1, \dots, R_k\}$ ,  $\cup_{i=1}^k R_i = I$ . The total coding length of the image  $I$  is

$$L_{w,\varepsilon}^S(\mathcal{R}) \doteq \sum_{i=1}^k L_{w,\varepsilon}(R_i) + \frac{1}{2}B(R_i). \quad (7)$$

Here, the boundary term is scaled by a half because we only need to represent the boundary between any two regions once. The optimal segmentation of  $I$  is the one that minimizes (7). Finding this optimal segmentation is, in general, a combinatorial task, but we can often do so using an *agglomerative* process.

To initialize the optimization process, similar to [12], we utilize an oversegmentation step to initialize the optimization by *superpixels*.<sup>5</sup> A superpixel is a small region in the image that does not contain strong edges in its interior. Superpixels provide a coarser quantization of an image than the underlying pixels, while respecting strong edges between the adjacent homogeneous regions. There are several methods that can be used to obtain a superpixel initialization, including those of Mori et al. [18], Felzenszwalb and Huttenlocher [3], and Ren et al. [11]. We have compared the three methods in the experiment and found that [18] works well for our purposes.

Given an oversegmentation of the image, at each iteration, we find the pair of regions  $R_i$  and  $R_j$  that will maximally decrease (7) if merged:

$$\begin{aligned} (R_i^*, R_j^*) &= \operatorname{argmax}_{R_i, R_j \in \mathcal{R}} \Delta L_{w,\varepsilon}(R_i, R_j), \quad \text{where} \\ \Delta L_{w,\varepsilon}(R_i, R_j) &\doteq L_{w,\varepsilon}^S(\mathcal{R}) - L_{w,\varepsilon}^S((\mathcal{R} \setminus \{R_i, R_j\}) \cup \{R_i \cup R_j\}) \\ &= L_{w,\varepsilon}(R_i) + L_{w,\varepsilon}(R_j) - L_{w,\varepsilon}(R_i \cup R_j) \\ &\quad + \frac{1}{2}(B(R_i) + B(R_j) - B(R_i \cup R_j)). \end{aligned} \tag{8}$$

$\Delta L_{w,\varepsilon}(R_i, R_j)$  essentially captures the difference in the lossy coding lengths of the texture regions  $R_i$  and  $R_j$  and their boundaries before and after the merging. If  $\Delta L > 0$ , we merge  $R_i^*$  and  $R_j^*$  into one region, and repeat this process, continuing until the coding length  $L_{w,\varepsilon}^S(\mathcal{R})$  can not be further reduced.

To model the spatial locality of textures, we further construct a *region adjacency graph* (RAG):  $\mathcal{G} = (\mathcal{V}, \mathcal{E})$ . Each vertex  $v_i \in \mathcal{V}$  corresponds to region  $R_i \in \mathcal{R}$ , and the edge  $e_{ij} \in \mathcal{E}$  is present if and only if regions  $R_i$  and  $R_j$  are adjacent in the image. To perform image segmentation, we simply apply a constrained version of the above agglomerative procedure – only merging regions that are adjacent in the image.

### 3.2 A Hierarchical Implementation

The above region-merging scheme is based on the assumption of a fixed texture window size, and clearly cannot effectively deal with regions or superpixels that are very small and/or thin. In such cases, the majority or all texture windows will intersect with the boundary of the regions. We say that a region  $R$  is *degenerate* w.r.t. window size  $w$  if  $\mathcal{I}_w(R) = \emptyset$ . For such a region, the  $w$ -neighborhoods of all pixels will contain pixels from other regions, and so  $\hat{\boldsymbol{\mu}}$  and  $\hat{\Sigma}$  cannot be reliably estimated. These regions are degenerate precisely because of the window size; for any  $w$ -degenerate region  $R$ , there is  $1 \leq w' < w$  such that  $\mathcal{I}_{w'}(R) \neq \emptyset$ .

<sup>5</sup> One could assume each pixel (and its windowed texture vector) belongs to a group of its own. However, in this case, texture windows of any size greater than one will (initially) intersect other adjacent regions (i.e., other neighboring pixels).



We say that  $R$  is *marginally nondegenerate* w.r.t. window size  $w$  if  $\mathcal{I}_w(R) \neq \emptyset$  and  $\mathcal{I}_{w+2}(R) = \emptyset$ . To deal with these degenerate regions, we propose to use a hierarchy of window sizes. Starting from the largest window size, we recursively apply the above scheme with ever smaller window sizes till all degenerate regions have been merged with their adjacent ones. In this paper, we start from  $7 \times 7$  and reduce to  $5 \times 5$ ,  $3 \times 3$ , and  $1 \times 1$ . For segmentation at smaller windows sizes, our scheme only allows adjacent regions to be merged if at least one of the regions is marginally nondegenerate.

Notice that at a fixed window size, the region-merging process is similar to the CTM approach proposed in [12]. Nevertheless, the new coding length function and hierarchical implementation give much more accurate approximation to the true image entropy and hence lead to much better segmentation results (see Section 4). We refer to our overall algorithm as *Texture and Boundary Encoding-based Segmentation (TBES)*.<sup>6</sup> On a Quad-Core Intel Xeon 2.5GHz machine, the superpixel initialization using the method of [18] takes roughly five minutes and our MATLAB implementation of TBES takes about ten minutes per image.

## 4 Experiments

In this section, we conduct extensive evaluation to validate the performance of our method. We first describe our experimental setup, and then show both qualitative and quantitative results on images from the publicly available Berkeley Segmentation Dataset (BSD).<sup>7</sup>

To obtain quantitative evaluation of the performance of our method we use three metrics for comparing pairs of image segmentations: the *probabilistic Rand index* (PRI) [20], the *variation of information* (VOI) [21], and the *precision and recall* of boundary pixels [6].<sup>8</sup> In cases where we have multiple ground-truth segmentations, to compute a given metric for a test segmentation, we simply average the results of the metric between the test segmentation and each ground-truth segmentation. With multiple ground-truth segmentations for an image we can also estimate the human performance w.r.t. these metrics by treating each ground-truth segmentation as a test segmentation and computing the metrics w.r.t. the other ground-truth segmentations.

To apply TBES to a natural image, we must choose the quantization level  $\varepsilon$ . As Figure 4 shows, a given image can have multiple plausible segmentations. We seek to find  $\varepsilon^*$  that tends to best match with human segmentation. To determine  $\varepsilon^*$  we run TBES on each of the 100 test images in BSD for sixteen choices of  $\varepsilon$  ranging from  $\varepsilon = 25$  to  $\varepsilon = 400$ . We then choose  $\varepsilon$  that obtains the best average performance w.r.t. the various metrics. In our experiments we found that the

<sup>6</sup> Detailed pseudocode for our TBES algorithm is available in our technical report [19].

<sup>7</sup> Please refer to our website for segmentation results on all images of the BSD, as well as additional experiments on the MSRC Object Recognition Database.

<sup>8</sup> We use the harmonic mean of precision and recall, known as the *global F-measure*, as a useful summary score for boundary precision and recall.

choice of  $\varepsilon^* = 150$  results in the best balance between the PRI and VOI metrics, so for all our subsequent experiments, we use this choice of  $\varepsilon$ .

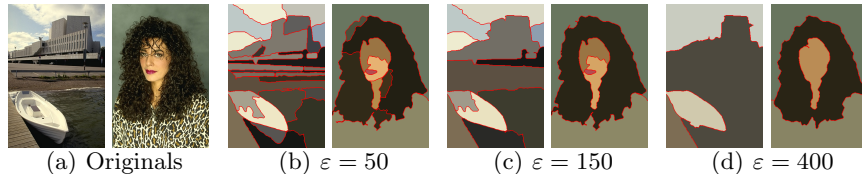


**Fig. 4.** (color) Results of TBES on two images for varying choices of  $\varepsilon$ .

The Berkeley Segmentation Dataset consists of 300 natural images, each of which has been hand segmented by multiple human subjects. Figure 6 illustrates some representative segmentation results. We compare the performance of our method to five *publicly available* image segmentation methods, which we refer to as “CTM” [12], “MS” [4], “NC” [2], “UCM” [6], and “F&H” [3], respectively. Table 2 and Figure 5 summarize the performance of our method based on the various metrics for the BSD: the indices PRI and VOI in Table 2 are used to evaluate goodness of the regions; and the precision-recall curve and F-measure in Figure 5 evaluate the segmentation boundaries.

**Table 2.** Comparison of PRI and VOI for various algorithms on the BSD.

Index / Method	Human	TBES ( $\varepsilon = 150$ )	CTM	MS	NC	UCM	F&H
PRI (Higher is better)	0.87	<b>0.80</b>	0.76	0.78	0.75	0.77	0.77
VOI (Lower is better)	1.16	<b>1.76</b>	2.02	1.83	2.18	2.11	2.15

Notice that in Table 2, for both indices, our method achieves the best performance compared to all popular segmentation methods. It is also surprising that it does so with a fixed  $\varepsilon$  whereas CTM needs to rely on a heuristic adaptive scheme. For our segmentation results, if we could choose the best  $\varepsilon$  adaptively for each image to optimize the PRI index, the average PRI over the entire database would become 0.849; similarly for the VOI index, using the best  $\varepsilon$  for each image brings this index down to 1.466, both strikingly close to that of human segmentation. This suggests there is still plenty of room to improve our method by designing better schemes for choosing  $\varepsilon$  adaptively.

## 5 Conclusion

We have proposed a novel method for natural image segmentation. The algorithm uses a principled information-theoretic approach to combine cues of image texture and boundaries. In particular, the texture and boundary information of

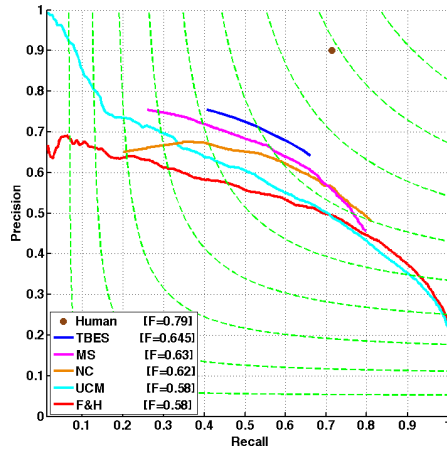


**Fig. 5.** (color) Precision vs. Recall of boundaries on the BSD. The green lines are level sets of the F-measure, ranging from 0.1 (lower left) to 0.9 (upper right). Our method (TBES) is closest to human performance (brown dot), achieving an F-measure of 0.645.

each texture region is encoded using a Gaussian distribution and adaptive chain code, respectively. The partitioning of the image is sought to achieve the maximum lossy compression using a hierarchy of window sizes. Our experiments have validated that this purely objective and simple criterion achieves state-of-the-art segmentation results on a publicly available image database, both qualitatively and quantitatively.

## References

1. Leclerc, Y.: Constructing Simple Stable Descriptions for Image Partitioning. *IJCV* **3** (1989) 73–102
2. Shi, J., Malik, J.: Normalized cuts and image segmentation. In: *Proceedings of the IEEE Conference on Computer Vision and Pattern Recognition (CVPR)*. (1997)
3. Felzenszwalb, P.F., Huttenlocher, D.P.: Efficient graph-based image segmentation. *International Journal of Computer Vision (IJCV)* **59**(2) (2004) 167–181
4. Comanicu, D., Meer, P.: Mean shift: A robust approach toward feature space analysis. *IEEE Transactions on Pattern Analysis and Machine Intelligence (PAMI)* **24** (2002) 603–619
5. Fua, P., Hanson, A.J.: An Optimization Framework for Feature Extraction. *Machine Vision and Applications* **4** (1991) 59–87
6. Arbelaez, P.: Boundary extraction in natural images using ultrametric contour maps. In: *Workshop on Perceptual Organization in Computer Vision*. (2006)
7. Ren, X., Fowlkes, C., Malik, J.: Learning probabilistic models for contour completion in natural images. *IJCV* **77** (2008) 47–63
8. Tu, Z., Zhu, S.: Image segmentation by data-driven Markov Chain Monte Carlo. *PAMI* **24**(5) (2002) 657–673

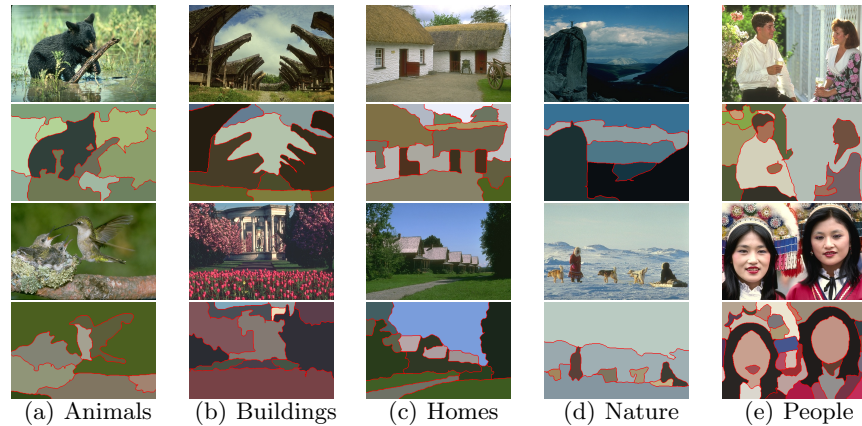


**Fig. 6.** (color) Qualitative results of our algorithm on various kinds of images from BSD with a fixed  $\varepsilon = 150$ . For each result, the top is the original image, and the bottom is a segmentation image where each region is colored by its mean color.

9. Kim, J., Fisher, J., Yezzi, A., Cetin, M., Willsky, A.: A nonparametric statistical method for image segmentation using information theory and curve evolution. *PAMI* **14**(10) (2005) 1486–1502
10. Yu, S.: Segmentation induced by scale invariance. In: *CVPR*. (2005)
11. Ren, X., Fowlkes, C., Malik, J.: Scale-invariant contour completion using condition random fields. In: *ICCV*. (2005)
12. Yang, A., Wright, J., Ma, Y., Sastry, S.: Unsupervised segmentation of natural images via lossy data compression. *Computer Vision and Image Understanding* **110**(2) (2008) 212–225
13. Ma, Y., Derksen, H., Hong, W., Wright, J.: Segmentation of multivariate mixed data via lossy coding and compression. *PAMI* **29**(9) (2007) 1546–1562
14. Martin, D., Fowlkes, C., Tal, D., Malik, J.: A Database of Human Segmented Natural Images and its Application to Evaluating Segmentation Algorithms and Measuring Ecological Statistics. In: *ICCV*. (2001)
15. Levina, E., Bickel, P.J.: Texture synthesis and non-parametric resampling of random fields. *Annals of Statistics* **34**(4) (2006) 1751–1773
16. Efros, A., Leung, T.: Texture synthesis by non-parametric sampling. In: *ICCV*. (1999)
17. Liu, Y.K., Zalik, B.: Efficient chain code with Huffman coding. *Pattern Recognition* **38**(4) (2005) 553–557
18. Mori, G., Ren, X., Efros, A., Malik, J.: Recovering human body configurations: combining segmentation and recognition. In: *CVPR*. (2004)
19. Rao, S., Mobahi, H., Yang, A., Sastry, S., Ma, Y.: Natural image segmentation with adaptive texture and boundary encoding. Technical Report UILU-ENG-09-2211 DC-244, UIUC (2009)
20. Rand, W.M.: Objective criteria for the evaluation of clustering methods. *Journal of the American Statistical Association* **66**(336) (1971) 846–850
21. Meila, M.: Comparing clusterings: An axiomatic view. In: *Proceedings of the International Conference on Machine Learning*. (2005)